Journal of Biomedical Optics

BiomedicalOptics.SPIEDigitalLibrary.org

Feasibility of using optical coherence tomography to detect acute radiation-induced esophageal damage in small animal models

Pouya Jelvehgaran
Daniel Martijn de Bruin
F. Javier Salguero
Gerben Roelof Borst
Ji-Ying Song
Ton G. van Leeuwen
Johannes F. de Boer
Tanja Alderliesten
Marcel van Herk

SPIE.

Pouya Jelvehgaran, Daniel Martijn de Bruin, F. Javier Salguero, Gerben Roelof Borst, Ji-Ying Song, Ton G. van Leeuwen, Johannes F. de Boer, Tanja Alderliesten, Marcel van Herk, "Feasibility of using optical coherence tomography to detect acute radiation-induced esophageal damage in small animal models," *J. Biomed. Opt.* **23**(4), 046004 (2018), doi: 10.1117/1.JBO.23.4.046004.

Feasibility of using optical coherence tomography to detect acute radiation-induced esophageal damage in small animal models

Pouya Jelvehgaran,[a,b,c,*] Daniel Martijn de Bruin,[a,d] F. Javier Salguero,[e] Gerben Roelof Borst,[e] Ji-Ying Song,[f] Ton G. van Leeuwen,[a] Johannes F. de Boer,[c] Tanja Alderliesten,[b] and Marcel van Herk[a,g]
[a]Academic Medical Center, Department of Biomedical Engineering and Physics, Amsterdam, The Netherlands
[b]Academic Medical Center, Department of Radiation Oncology, Amsterdam, The Netherlands
[c]Institute for Laser Life and Biophotonics Amsterdam, Department of Physics and Astronomy, Amsterdam, The Netherlands
[d]Academic Medical Center, Department of Urology, Amsterdam, The Netherlands
[e]The Netherlands Cancer Institute, Department of Radiation Oncology, Amsterdam, The Netherlands
[f]The Netherlands Cancer Institute, Department of Experimental Animal Pathology, Amsterdam, The Netherlands
[g]University of Manchester, Institute of Cancer Sciences, Manchester, United Kingdom

Abstract. Lung cancer survival is poor, and radiation therapy patients often suffer serious treatment side effects. The esophagus is particularly sensitive leading to acute radiation-induced esophageal damage (ARIED). We investigated the feasibility of optical coherence tomography (OCT) for minimally invasive imaging of the esophagus with high resolution (10 μm) to detect ARIED in mice. Thirty mice underwent cone-beam computed tomography imaging for initial setup assessment and dose planning followed by a single-dose delivery of 4.0, 10.0, 16.0, and 20.0 Gy on 5.0-mm spots, spaced 10.0 mm apart in the esophagus. They were repeatedly imaged using OCT up to three months postirradiation. We compared OCT findings with histopathology obtained three months postirradiation qualitatively and quantitatively using the contrast-to-background-noise ratio (CNR). Histopathology mostly showed inflammatory infiltration and edema at higher doses; OCT findings were in agreement with most of the histopathological reports. We were able to identify the ARIED on OCT as a change in tissue scattering and layer thickness. Our statistical analysis showed significant difference between the CNR values of healthy tissue, edema, and inflammatory infiltration. Overall, the average CNR for inflammatory infiltration and edema damages was 1.6-fold higher and 1.6-fold lower than for the healthy esophageal wall, respectively. Our results showed the potential role of OCT to detect and monitor the ARIED in mice, which may translate to humans. [DOI: 10.1117/1.JBO.23.4.046004]

Keywords: optical coherence tomography; esophagus; image-guided radiation therapy; acute radiation-induced esophageal damage; small animal models; lung cancer.

Paper 170727RR received Nov. 11, 2017; accepted for publication Mar. 26, 2018; published online Apr. 12, 2018.

1 Introduction

For patients with lung cancer, advanced image-guided radiation therapy (RT) could significantly improve clinical outcomes by controlling the lung tumor with radiation dose escalation or acceleration.[1] Lung cancer RT is, however, hampered by toxicity to nearby healthy organs, such as the esophagus, which is particularly vulnerable to irradiation. Acute radiation-induced esophageal damage (ARIED) or acute esophagitis can be a dose-limiting factor during head and neck cancer and lung cancer RT.[2–7] Acute radiation-induced damages appear within three months after RT, and late radiation-induced damages occur more than three months postirradiation.[8,9] ARIED arises in most patients treated with lung and thoracic RT since the gastrointestinal tract is often close to the primary tumor or tumor-bearing lymph nodes.[5,10–12] ARIED may result in reduced food intake, feeding tube requirement, fistula formation, hospitalization, and surgical intervention. These complications are often dose-limiting, necessitating lowering treatment dose and as such hamper the local tumor control.[13,14] Improved knowledge of the effects of irradiation on the organs at risk is paramount to allow better optimization of the balance between tumor control and damage to the neighboring organs. Currently, there are limited means to determine ARIED, such as white light endoscopy (WLE) and positron emission tomography (PET).[15] The presumed relation between the dose distribution and patient symptoms is so far mainly based on toxicity scored in clinical practice, without visualizing ARIED.[13,16] One study found that the expansion of the esophagus on computed tomography (CT) images has potential as an objective measure of toxicity.[14] If we could detect and monitor ARIED, we would be able to modify RT and, thereby, prevent complications avoiding treatment interruptions, which would enhance the quality of life of patients.

Optical coherence tomography (OCT) is a minimally invasive depth-resolved imaging modality to obtain cross-sectional images with high resolution (10 μm). OCT acquires backscattered near-infrared light from tissue. The depth of OCT imaging is limited to 2.0 to 3.0 mm because of light–tissue interaction.[17,18] Cylindrical catheters with single rotating optical fibers are capable of scanning the esophageal wall surface over a length of 6 cm.[19–24] A probe-based OCT imaging session can

*Address all correspondence to: Pouya Jelvehgaran, E-mail: p.jelvehgaran@amc.uva.nl

be combined with a standard WLE procedure for minimally invasive diagnosis. More recently, a tethered capsule endomicroscopy technique was integrated in a pill-like imaging device meant for voluntary swallowing, which is capable of cross-sectional OCT imaging of the whole esophagus without sedation and minimal burden to patients.[25–27] In contrast to endoscopy, OCT creates three-dimensional (3-D) depth-resolved architectural microscopic images that may be spatially correlated with histopathology. We hypothesize that OCT may detect radiation-induced damage in the esophagus, e.g., by quantifying changes in light scattering of tissue. Cellular changes, such as apoptosis, necrosis, and inflammation postirradiation, are known to change light scattering properties.[28,29]

In this study, we qualitatively and quantitatively investigated the feasibility of OCT to detect ARIED preclinically in mice. We compared toxicity based on histopathology reports with OCT findings.

2 Materials and Methods

2.1 *Mice and Ethical Guidelines*

Our study on mice adhered to the rules of the Dutch animal experimentation act, approved by the animal experimentation ethics committee. Mice were specific pathogen free (SPF), female, between the age of 8 and 10 weeks, and of FVB strain. They were ordered from a commercial vendor and directly delivered to our small animal facility. Upon arrival, we accommodated them in disposable filter-top individually ventilated cages. Mice had free access to acidified drinking water and standardized 4.0% fat mouse chow diet. By the end of the experiment (three months postirradiation), mice were euthanized according to the protocol using a lethal injection of Nembutal. Humane endpoint criteria to euthanize mice were defined as more than 15.0% body weight loss or signs of distress, such as hair loss.

2.2 *Anesthetic Agent*

We used Hypnorm/Dormicum anesthetic injection (0.1 mg/gr) to sedate the mice for the cone-beam CT, dose planning, and dose delivery, which takes up to 40 min per mouse at the higher dose levels. Mice anesthetized in this way are expected to remain asleep for about 2 h, which also facilitated the first OCT imaging 1-h postirradiation. We used intravascular Ketamine/Xylazine injection (0.1 mg/gr), which was effective for about 45 min, during the remaining OCT imaging sessions. Anesthetized mice were placed on a heating pad to maintain a normal body temperature during imaging/dose delivery. A heating lamp was used during recovery.

2.3 *Imaging Equipment*

2.3.1 *Cone-beam CT imaging and dose delivery*

To irradiate the mice, we used a dedicated image-guided small animal irradiation system (X-RAD 225Cx, Precision X-ray Inc., North Branford, Connecticut) that includes cone-beam CT image guidance, planar x-ray imaging, and dose delivery.[30]

2.3.2 *OCT imaging*

We obtained endoscopic *in vivo* OCT images of the esophagus using a commercially available C7-XR™ intravascular imaging system (St. Jude Medical, St. Paul, Minnesota). This device is designed for intravascular imaging and, therefore, compatible with the small diameter of the mouse esophagus. The OCT imaging system used a C7 Dragonfly™ intravascular imaging probe (St. Jude Medical, St. Paul, Minnesota), which is a rotating fiber capable of longitudinal pullback. The probe has an outer diameter of 0.9 mm and produces images with an axial resolution of 15.0 μm and lateral resolution of 30 to 35 μm.[23,24]

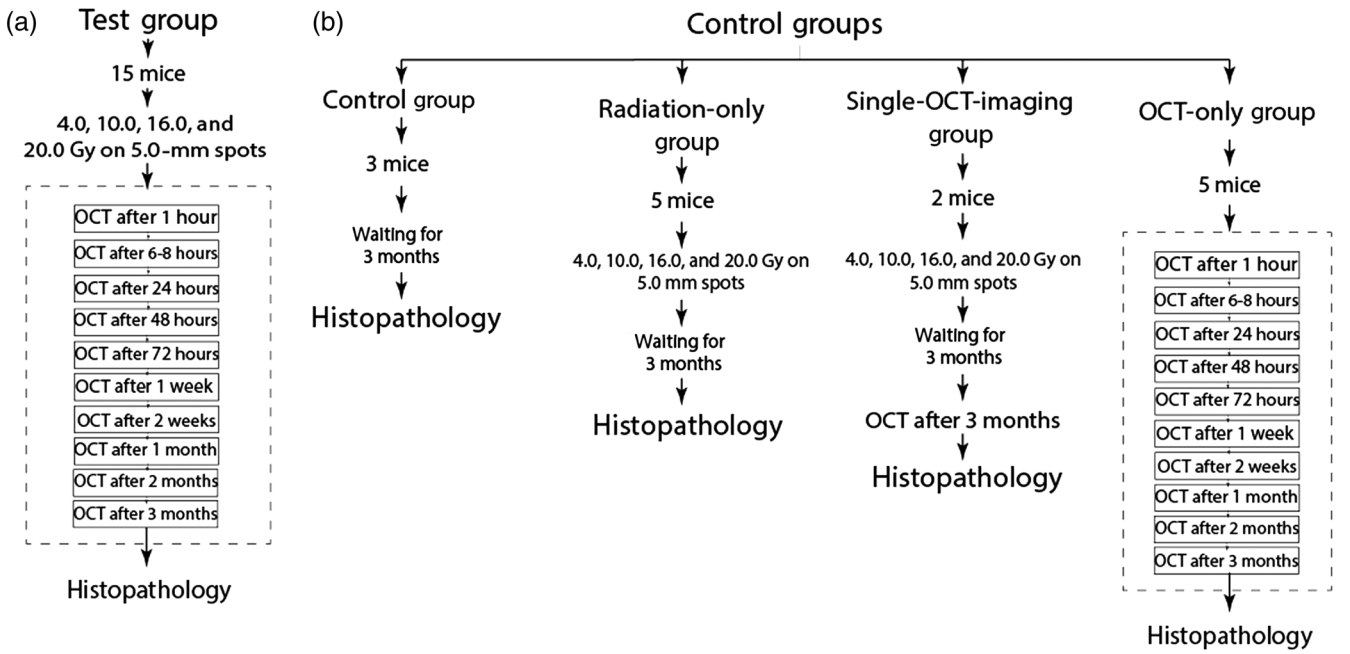

Fig. 1 Flowchart demonstrating all the steps for the mice (a) in the test group and (b) in the control, radiation-only, single-OCT-imaging, and OCT-only groups.

2.3.3 *Histopathology visualization*

Esophagi of euthanized mice were fixed in EAF (ethanol/acetic acid/formaldehyde/saline 40:5:10:45 v/v) and embedded horizontally in paraffin. Sagittal sections were made at 2 μm from the paraffin blocks and stained with hematoxylin and eosin. For the histopathology analysis, we used a Zeiss Axioskop2 Plus microscope (Carl Zeiss Microscopy, Oberkochen, Germany). Digital microscopic images were taken with a Zeiss AxioCam HRc digital camera and processed with AxioVision 4 software (both Carl Zeiss Vision, Munich, Germany).

2.4 *Methods*

2.4.1 *Colocalization of OCT images with histopathology*

We had four dose locations; however, because of the difficulties to define these exact locations in the histopathology specimen, we divided the esophageal specimen into three anatomical regions. We subsequently also divided the sagittal OCT esophageal wall image into these anatomical regions and visually matched the histopathology results to the OCT images. The trachea bifurcation was used as anatomical landmark to align 3-D OCT images.

2.4.2 *Data analysis and statistical analysis*

Guided by the histopathology results obtained at three months postirradiation, we visually inspected the 3-D OCT images individually to detect esophageal damages. Esophageal damages were identified by changes in tissue scattering properties and layer thickness. Registration of the OCT and the histopathology is qualitative, based on the location along the length of the esophagus. We used in-house developed software (Worldmatch)[31] for the visualization and processing of our data to better detect esophageal layers and damages. We evaluated the visibility of such damage quantitatively by calculating the contrast-to-background-noise ratio (CNR).[32] Refer to the Appendix for a detailed description of the methods.

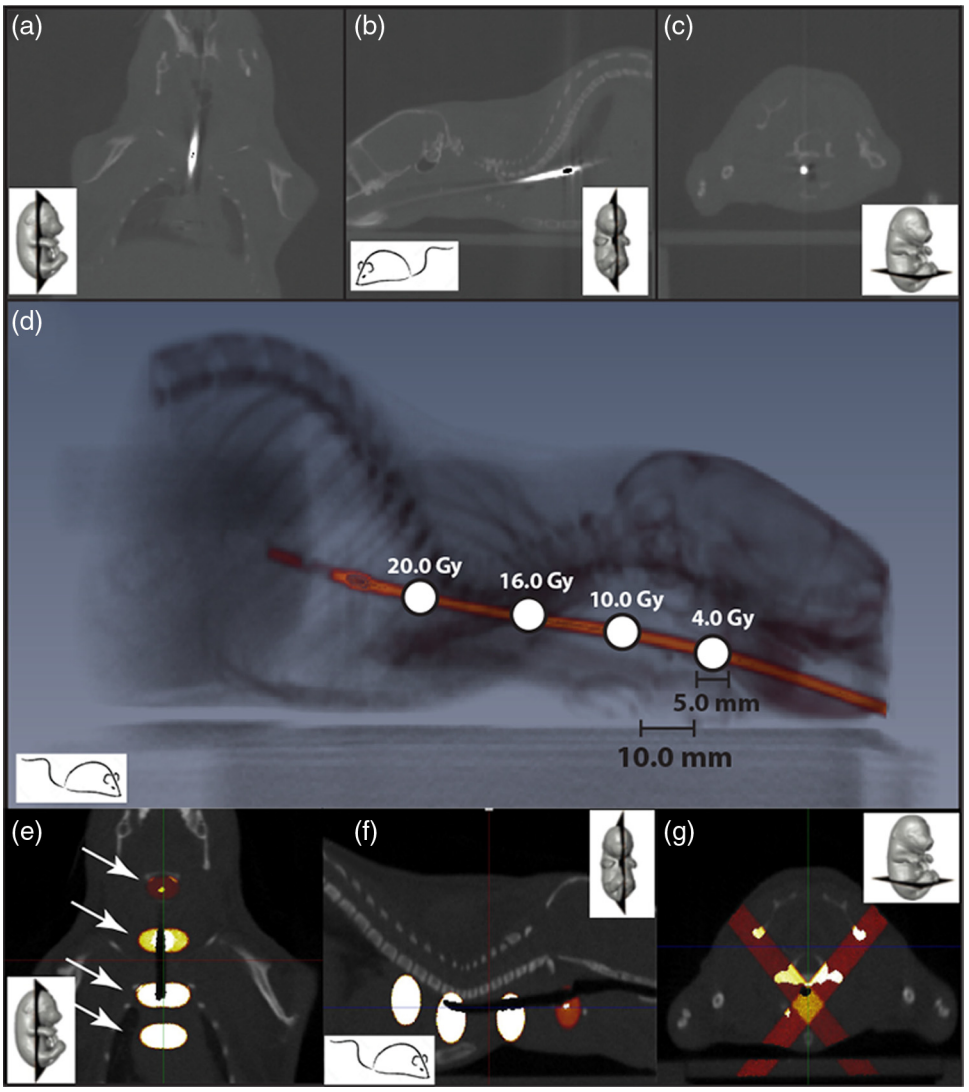

Fig. 2 (a–c) These cone-beam CT images illustrate the visibility of the OCT probe filled with diluted CT contrast in coronal, sagittal, and axial planes, respectively. (d) A 3-D reconstruction of the cone-beam CT shows the visibility of the OCT probe and illustrates the dose planning. (e–g) These images show the dose distribution (white arrows) in coronal, sagittal, and axial planes overlaid on the planning cone-beam CT, respectively.

We also measured the distance between the muscularis mucosa and lamina propria of edema and healthy esophageal tissues to evaluate the visibility of edema quantitatively. We used repeated measures analysis of variance (ANOVA) to evaluate the differences in distances and CNR values (Appendix).

2.4.3 *Experimental protocol*

We randomly divided 30 SPF FVB mice into five experimental groups (one test and four control groups), irradiated them once, and imaged for three months. The OCT-only group was compared with the radiation-only group to differentiate between probe insertion- and radiation-related damages in the esophagus. The single-OCT-imaging group of two mice was used to check if single-OCT probe insertion may cause significant damage.

After applying anesthesia, we held the mice by the scruff of the neck in one hand while gently inserting the OCT probe to a standardized level with the other hand. To avoid damaging the tongue, the tongues of the mice were extended and visible during insertion. We advanced the OCT probe down to the stomach opening, where we sensed a bit of an impasse. Inserting the OCT probe up to standardized length marking reduced the risk of probe-induced damage or incomplete tissue coverage with too deep or too shallow insertions, respectively. The OCT probe was disinfected with ethanol after each insertion.

The mice (test, radiation-only, and single-OCT-imaging groups) underwent cone-beam CT imaging for initial setup assessment and dose planning, followed by a single-dose delivery of 4.0, 10.0, 16.0, and 20.0 Gy on four 5.0-mm spots, spaced 10.0 mm apart (Figs. 1 and 2), with the higher doses delivered distally. Irradiation used two orthogonal circular beams at 45 deg. The imaging dose was about 0.7 and 0.5 cGy on the skin and at a 10.0-mm depth, respectively. The OCT probe, preloaded with CT contrast diluted 1:3 in water, was inserted prior to cone-beam CT scanning, helping to localize the esophagus in cone-beam CT images for treatment planning and dose delivery (Fig. 2).

Three months postirradiation, each mouse was euthanized, and we dissected the esophagus and stomach attached together. Having the stomach in the specimen helped us to identify proximal and distal esophagus locations and better decide where to cut the tissue for histopathology analysis.

3 Results

3.1 *Histopathology Findings*

Figure 3 demonstrates esophageal damages at three months postirradiation in histopathology and OCT. Table 1 summarizes the histopathology results of all the mice in proximal, middle, and distal esophagus locations for all experimental groups. We found inflammatory infiltration in the test group (4 out of 15 mice) and the radiation-only group (one out of five mice). No incidence of inflammatory infiltration was found in the OCT-only, single-OCT imaging, and control groups. Edema was seen in the test group (9 out of 15 mice) and the OCT-only group (2 out of 5 mice). No incidence of edema was found in the radiation-only, single-OCT imaging, and control groups.

No mice had to be euthanized at humane endpoint during our experiment. In the test group, 27.2% of the edema was found in the proximal esophagus (at low dose) and 36.4% each in the middle and distal esophagus. In the OCT-only group, 28.6%

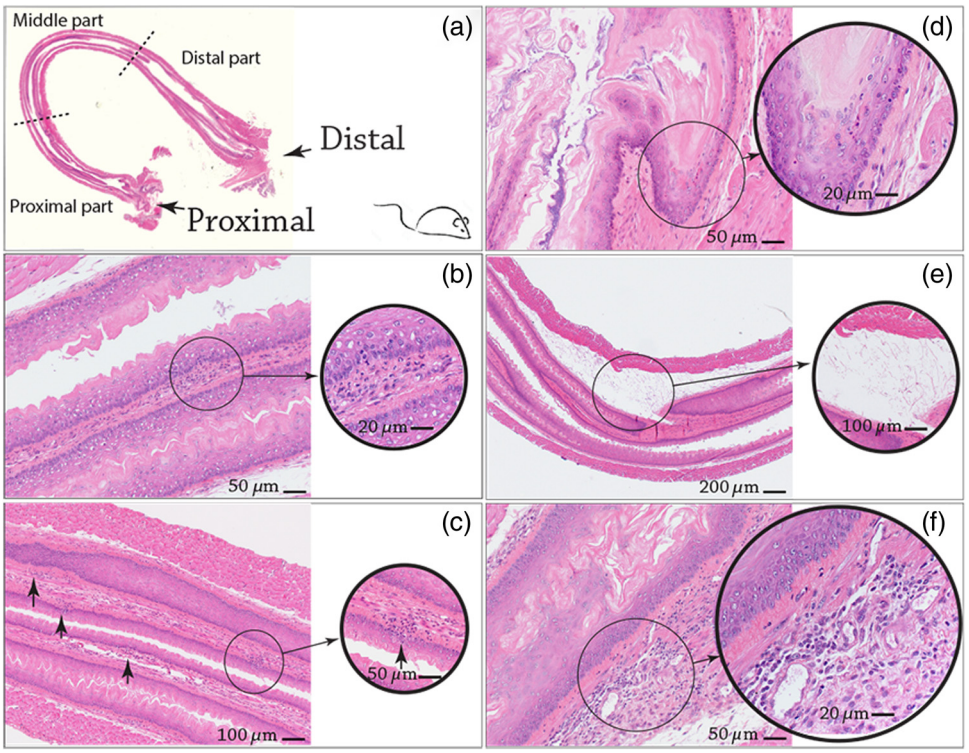

Fig. 3 Histopathology and OCT results showing ARIED in mice. Specimens were cut sagittally: (a) a longitudinal section of the mouse esophagus indicating proximal, middle, and distal parts, (b) focal inflammatory infiltration, (c) multifocal inflammatory infiltration, (d) dyskeratotic and degenerative cells, (e) edema, and (f) inflammatory infiltration and hypertrophy of the endothelial cell in the submucosa.

Table 1 Histopathology results showing ARIED in mice. Since for the single-OCT-imaging group no ARIED was observed at histopathology, this group is not included in this overview.

Group	Proximal esophagus	Middle esophagus	Distal esophagus
Test			
Mouse 1	—	Mildly increased collagen in the submucosa, mainly around small vessels with hypertrophy of the endothelial cells	—
Mouse 2	Inflammatory infiltrations in the submucosa and focally in the mucosa	Inflammatory infiltrations in the submucosa	Multifocal inflammatory infiltrations in the mucosa and submucosa
Mouse 3	—	—	—
Mouse 4	—	Mild edema in the submucosa	Small clusters of the squamous cells show dyskeratotic and degenerative changes and pyknosis at the surface of the mucosa
Mouse 5	Edema in the submucosa	—	Mild edema in the submucosa
Mouse 6	Mild edema with increased amount of collagen in the submucosa	Mild edema in the submucosa with increased amount of collagen around blood vessels	Mild edema in the submucosa with increased amount of collagen around blood vessels
Mouse 7	Degeneration (vacuolization) of the epithelial cells accompanied by the edema and inflammatory infiltrations in the mucosa	Mild edema in the submucosa	Inflammatory infiltrations in the submucosa with increased amount of collagen around blood vessels
Mouse 8	—	Local and mild degeneration (vacuolization) of the epithelial cells with mild inflammatory infiltrations	—
Mouse 9	—	—	Single apoptotic cells in the mucosa with mild increase of collagen in the submucosa
Mouse 10	—	—	Dilation of the blood vessels with mildly increased collagen in the mucosa/submucosa
Mouse 11	—	—	—
Mouse 12	—	—	—
Mouse 13	—	—	—
Mouse 14	—	Edema in the submucosa	Congestion of the blood vessels in the mucosa and submucosa with mild and focal inflammation and edema
Mouse 15	—	—	Locally increased cellularity in the lamina propria of the mucosa
OCT-only			
Mouse 1	—	—	—
Mouse 2	—	Dyskeratosis in a single cell	—
Mouse 3	Single apoptotic cell in the mucosa	—	Mild edema in the submucosa
Mouse 4	Mild edema in the submucosa	Mild edema in the submucosa	Mild edema in the submucosa
Mouse 5	Mild edema in the submucosa	Mild edema in the submucosa	Mild edema in the submucosa
Radiation-only			
Mouse 1	—	—	—

Table 1 (*Continued*).

Group	Proximal esophagus	Middle esophagus	Distal esophagus
Mouse 2	—	—	—
Mouse 3	—	—	—
Mouse 4	—	—	Local increased amount of collagen and newly formed blood vessels in the submucosa
Mouse 5	—	Focal inflammatory infiltrations in the mucosa	Mild degenerative changes (vacuolization) of the epithelial cells with mild inflammatory infiltrations in the mucosa and congestion in the submucosa
Control			
Mouse 1	—	—	—
Mouse 2	—	—	—
Mouse 3	—	—	Focal dyskeratosis of the epithelial cells and focal inflammatory in the mucosa
Mouse 4	—	—	—
Mouse 5	—	—	—

of the edema incidents occurred in both the proximal and middle esophagus; this was 42.8% in the distal part. In total (i.e., for the test and the OCT-only groups combined), the edema incidence was 27.8%, 33.3%, and 38.9% for the proximal, middle, and distal esophagus, respectively.

Inflammatory infiltration incidents in the radiation-only group were seen equally in the middle and distal esophagus with no incidence in the proximal part. In total (i.e., for the test and the radiation-only groups combined), 50.0% of all inflammatory infiltration incidents were distally located (high dose), with 37.5% and 12.5% of total incidents in the middle (intermediate dose) and proximal (low dose) parts of the esophagus, respectively [Fig. 9(a)]. Because most of the inflammatory infiltration was observed at the highest dose region, we concluded that inflammatory infiltration was a radiation-induced damage, while edema was independent of dose and most likely caused by OCT probe insertions.

3.2 *OCT Findings*

We solely looked for edema and inflammatory infiltration damages—as the major histopathology reported damages—in our OCT analysis. Guided by histopathology, we found that areas with inflammatory infiltration had high scattering regions that infiltrated/induced into either the mucosa or the submucosa, i.e., at one certain depth. Our quantitative analyses were solely performed for these regions, excluding high scattering signals elsewhere. Edema mostly had low scattering properties combined with swelling of the submucosal layer. The last OCT imaging time point—three months postirradiation and right before the mice were euthanized—was just before histopathology was performed. We found that 85.7% of the inflammatory infiltration and 81.3% of the edema reported in histopathology were detected in these OCT images.

Figure 4 shows an *in vivo* endoscopic OCT image of a healthy mouse esophagus that illustrates different layers (epithelium, lamina propria, muscularis mucosa, submucosa, and muscle layers). Figure 5(a) shows a healthy esophagus while Fig. 5(b) shows inflammatory infiltration in the distal esophagus and edema in the middle esophagus. Figure 6 shows *en-face* view of inflammatory infiltration (high scattering that infiltrates in mucosa or submocusa) and edema (low scattering with swelling) in the proximal and middle esophagus. Figure 7 shows the corresponding findings on inflammatory infiltration and edema in histopathology and OCT images. Figure 8 shows the edema and the inflammatory infiltration of a mouse from the test group at all OCT imaging time-points, to facilitate monitoring damages over time.

We quantitatively measured the differences between healthy tissue and edema in terms of the distance between the muscularis mucosa and lamina propria on OCT [Fig. 9(b)]. There was a statistically significant difference between the two groups ($p = 0.00025$). These distances for edema and healthy esophageal wall on average $\pm$ standard deviation were 0.9 ± 0.2 mm (range: 0.6 to 1.2 mm, median 1.0 mm) and 1.6 ± 0.5 mm (range: 1.1 to 2.7 mm, median 1.6 mm), respectively. On average, the distance between muscularis mucosa and lamina propria was 1.7-fold higher in edema than in the healthy esophageal wall.

Our quantitative analysis based on CNR differences between healthy esophageal wall, edema, and inflammatory infiltration at three months postirradiation is summarized in Fig. 9(c). There was a statistically significant difference among the three groups ($p = 0.00035$). On average, the CNR was 1.6-fold higher in inflammatory infiltration than in the healthy esophageal wall.

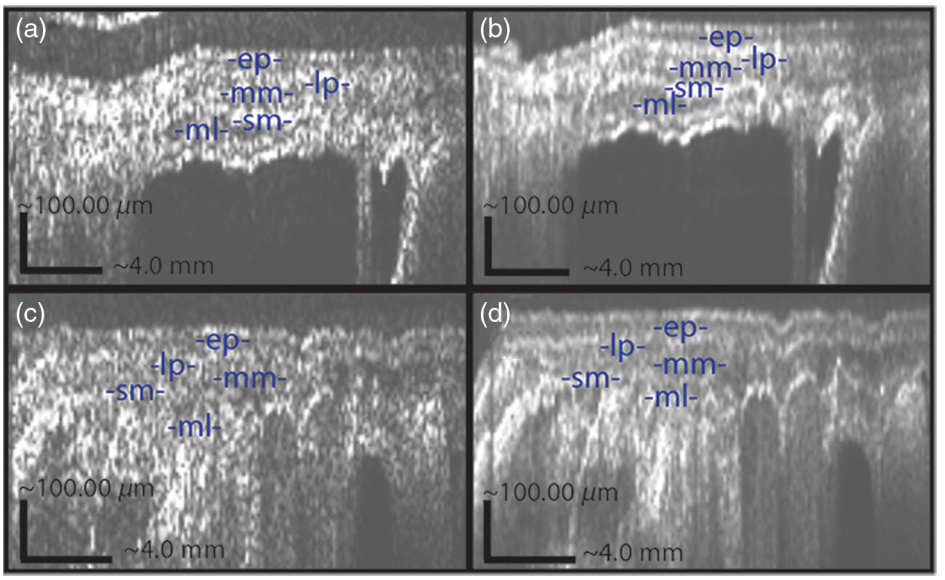

Fig. 4 OCT images of an *in vivo* normal esophageal wall in mice. Esophageal wall layers are indicated as: ep = epithelium, lp = lamina propria, mm = muscularis mucosa, sm = submucosa, and ml = muscle layers. (a) Axial plane (the image is unfolded to appear straight rather than circular), (b) axial plane (the images are averaged over three slices perpendicular to the view direction, to improve signal-to-noise ratio and therewith the visualization), (c) sagittal plane (note that sagittal view has inferior resolution due to the image acquisition procedure), and (d) axial view averaged over three slices perpendicular to the view direction.

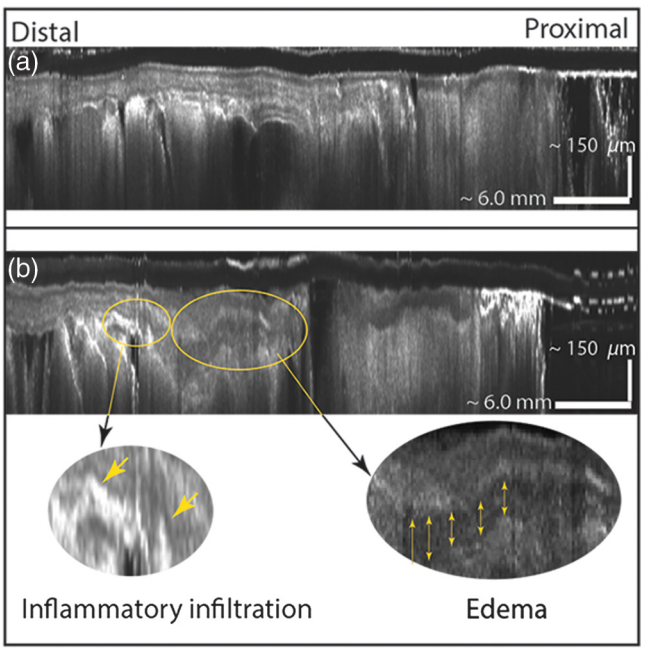

Fig. 5 (a) *In vivo* OCT image of a control mouse that shows no inflammatory infiltration and edema and (b) *in vivo* image of a mouse from the test group illustrating inflammatory infiltration in the distal esophagus and edema in the middle esophagus. The images are averaged over 21 slices perpendicular to the view direction.

The CNR of edema was 1.6-fold lower than the healthy esophageal wall. The CNRs for healthy esophageal wall, edema, and inflammatory infiltration on average ± standard deviation were 17.1 ± 6.2 (range: 8.7 to 27.6, median 15.1), 10.9 ± 5.0 (range: 4.0 to 19.5, median 10.4), and 28.0 ± 9.0 (range: 15.5 to 36.1, median 31.4), respectively.

Moreover, we calculated the CNR values of all inflammatory infiltration incidents observed at a subset of time-points [Fig. 9(d)]. The total average ± standard deviation of the calculated CNRs of the inflammatory infiltration damage was 53.6 ± 41.5 (range: 15.5 to 193.8, median 38.8), and this average CNR was 1.9-fold higher than the CNR of inflammatory infiltration after three months and 3.1-fold higher than the CNR of the healthy esophageal wall.

4 Discussion

In this study, we investigated ARIED as a function of dose using four increasing dose levels from the proximal to distal end of the esophagus. After irradiation, we imaged them for three months. Compared with the histopathology results acquired at three months after dose delivery, OCT was capable of detecting inflammatory infiltration and edema in mice as a change in light scattering and esophageal wall layer thickness compared to unirradiated mice. Our results suggest that inflammatory infiltration is a radiation-induced damage, while multiple OCT probe insertions caused edema. Edema caused expansion between the muscularis mucosa and lamina propria esophageal walls. Both changes were small but statistically significant on quantitative analysis. Single-OCT probe insertion was less damaging; hence, we saw no edema in the single-OCT-imaging group. The OCT probe insertion-induced edema should be much lower or absent in humans due to availability of dedicated esophageal OCT catheters that can be inserted in a deflated state[32] and because of the larger size of the organ.

Previous studies investigated the use of OCT in esophageal and radiation-induced damages,[20,33–46] the visibility of esophageal layers in OCT images, and the differentiation between healthy and cancerous esophagus.[39–41] Esophageal OCT has been used to detect Barrett's esophagus in various studies.[20,40,42,43] Some studies used functional OCT microvascular imaging for

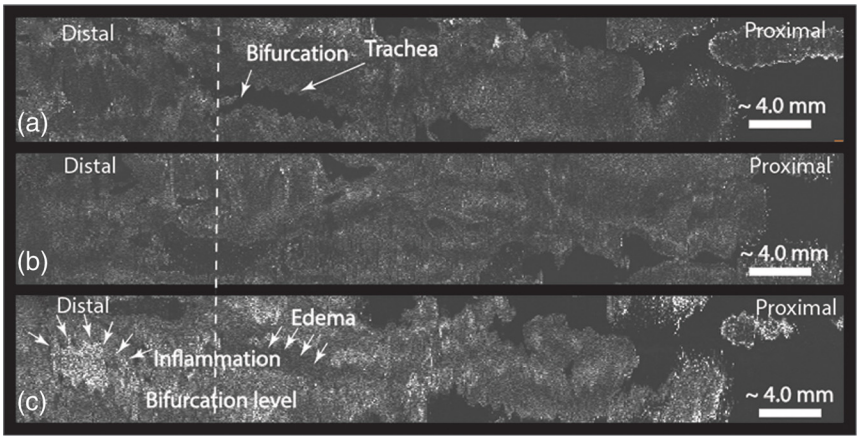

Fig. 6 (a) *En-face* illustration of an *in vivo* OCT image of a normal esophagus represents trachea and the bifurcation (~0.4-mm depth), (b) same at ~0.2-mm depth, and (c) illustrates edema in the middle esophagus and inflammatory infiltration in the distal esophagus (high-dose region) at about submucosal depth (~0.2-mm depth). The images are averaged over 21 slices perpendicular to the view direction, to improve signal-to-noise ratio and therewith the visualization.

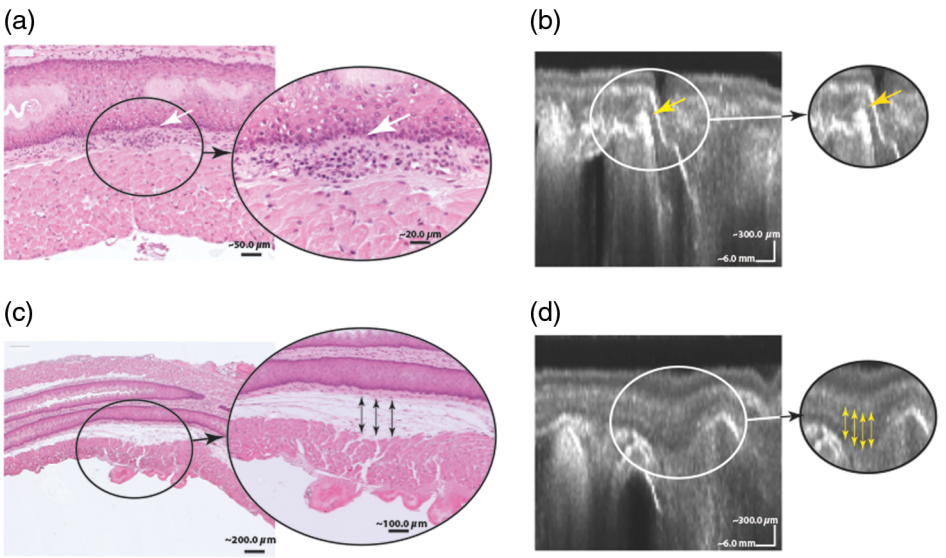

Fig. 7 (a, b) Corresponding inflammatory infiltration damages in the middle esophagus in histopathology and OCT. (c, d) Corresponding edema damages in the same region of the same mouse.

radiobiological monitoring of different radiation dose levels in pancreatic human tumor xenografts[47] and in head and neck cancer using multifunctional OCT in a clinical pilot study in patients.[48] Moreover, there are pilot patient studies reported on using microvascular OCT imaging with developed oral imaging probes to monitor late oral radiation-induced damages *in vivo*.[36,49] However, it is unknown whether we can directly compare these findings with dose response of the esophagus in mice.

Other side effects, such as ulceration, perforation, and fistula formation exist besides the ARIED reported here.[11,50] Edema and fistula formation are late RT complications that increase significantly with dose.[51] Also concurrent chemotherapy increases the risk of radiation-induced damages.[8,50] In this study, we solely focused on the acute dose-related toxicity and we did not use chemotherapy.

Although inflammatory infiltration was the main histopathologically reported incident in OCT images and appeared as a high scattering region, not all high scattering regions are due to inflammatory infiltration. We defined inflammatory infiltration as high scattering regions that infiltrated into the mucosa or submucosa. We found high scattering regions in almost all OCT images, including in the control group, which are not infiltrating into the upper esophageal layers (Fig. 10). We suspect that these regions may represent muscle tissue. There were also regions in OCT that looked like edema or inflammatory infiltration, which were not reported on histopathology analysis, suggesting that we may have undersampled the specimens. Because of the lack of histopathology validation, these regions were not analyzed in OCT images.

Histopathology results (Table 1) indicated that we only induced limited acute damage in the esophagi of the mice. We hypothesize that the small spot size and chosen dose levels may play a role. Studies in rats have shown that no histopathologic damage is associated with delivered dose up to 18.0 and <20.0 Gy to the cervical spinal cord.[52,53] However, in mice, esophageal radiation-induced damage at one week

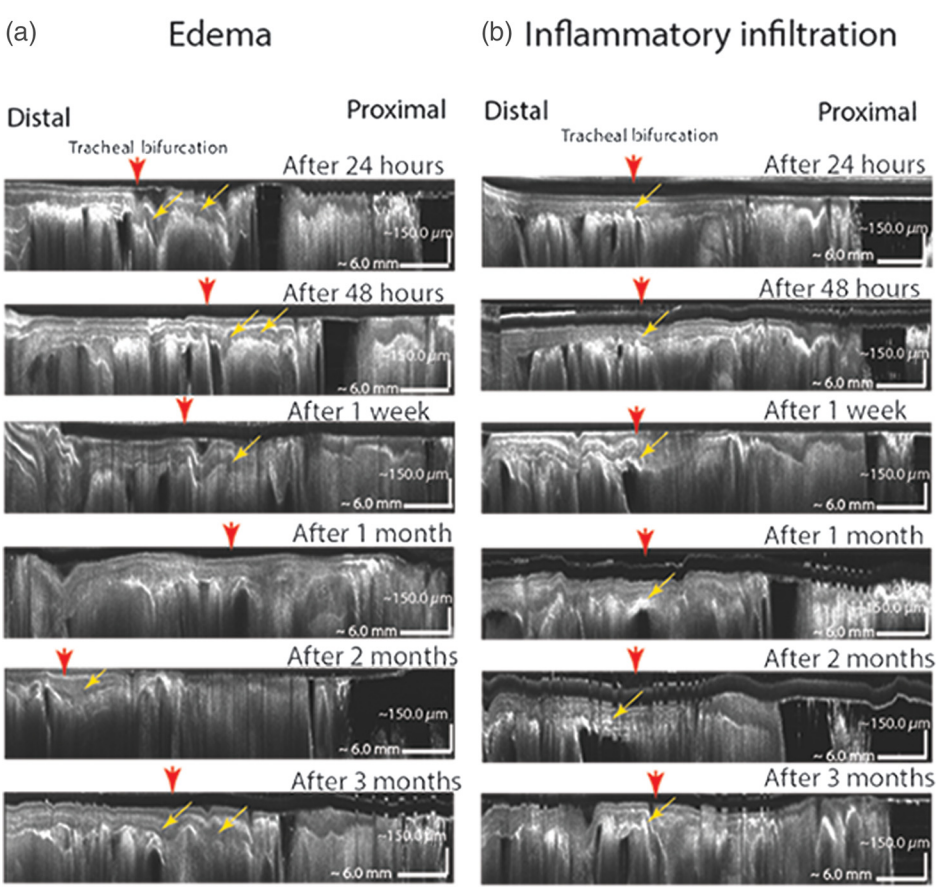

Fig. 8 (a) *In vivo* OCT images of edema in mouse 6 (test group) at 6 time-points postirradiation. The images are averaged over 21 slices perpendicular to the view direction. Yellow arrows point to the suspected edema in the submucosa. Red arrows indicate the tracheal bifurcation level as reference of the middle esophagus. (b) *In vivo* OCT images of inflammatory infiltration in mouse 8 (test group) at 6 time-points postirradiation. Yellow arrows point to the suspected inflammatory infiltration incidents. Red arrows indicate the tracheal bifurcation level as the reference of the middle esophagus.

postirradiation was reported when 30.0 Gy was delivered.[54] We delivered the maximum single dose of 20.0 Gy in a 0.5-mm spot to limit normal tissue toxicity outside the esophagus, prevent morbidity, and preserve the mice's physical condition for repeated imaging for three months. In view of uncertainties in the image-guided small animal irradiation system and/or biological effects limiting damage for small regions, our selected spot size may have been too small, and the small fields might also have caused us to miss damaged areas as a result of undersampling of the histopathology. Although for this study it was not feasible to address the undersampling by embedding the entire esophagus for all the mice because of the timely and expensive process, we could revisit this in the future. The assumed human esophageal tolerance for single fraction irradiation is 27 Gy, using an α/β ratio of 3 Gy^{-1}.[55] From our results, using a dose that is below that reported tolerance, we cannot conclude whether the radiobiological sensitivity of mice is different from humans. However, the esophageal wall layering of humans and mice is similar; therefore, our model is a reasonable choice for preclinical investigation. The esophagus is a serial organ[56] where damage to a single functional subunit may result in damaging the entire organ.[57] Therefore, the esophagus may show different results, in which case we would have a single irradiation spot compared to our findings for consecutive irradiation spots along the organ. However, modifying treatment parameters, such as the dose distribution, may prevent esophageal strictures.[4] Our experimental protocol was designed such that we investigated the ARIED with four dose levels per mice, using each mouse as its own control. A limitation of this setup is that we could not study whether there is a serial effect—where organ response is dependent on the length of the irradiated tissue.

Figure 6(a) shows the trachea in an *en-face* OCT image. The trachea often appeared as a serpentine organ because of nonuniform rotational distortion (NURD).[22,58–61] NURD depends on various parameters, such as catheter specifications and material, subject movement, specific path in the body during the pullback, and the pullback position.[58] The imaging artifacts caused by NURD, breathing, and probe movements in our study mainly affected the visual quality of the OCT images, resulting in difficulties to interpret some of the data.

Future work includes protocol modification to make sure that we induce more substantial ARIED and perform another small animal study. In future studies, one will be able to reduce the probability of edema formation in the mice by performing less OCT imaging. This can be followed by investigating the feasibility of OCT to detect and monitor ARIED in humans and *in vivo* in patients with lung cancer undergoing RT using a dedicated esophageal OCT system. We expect that our *in vivo* findings can be translated to humans because of the

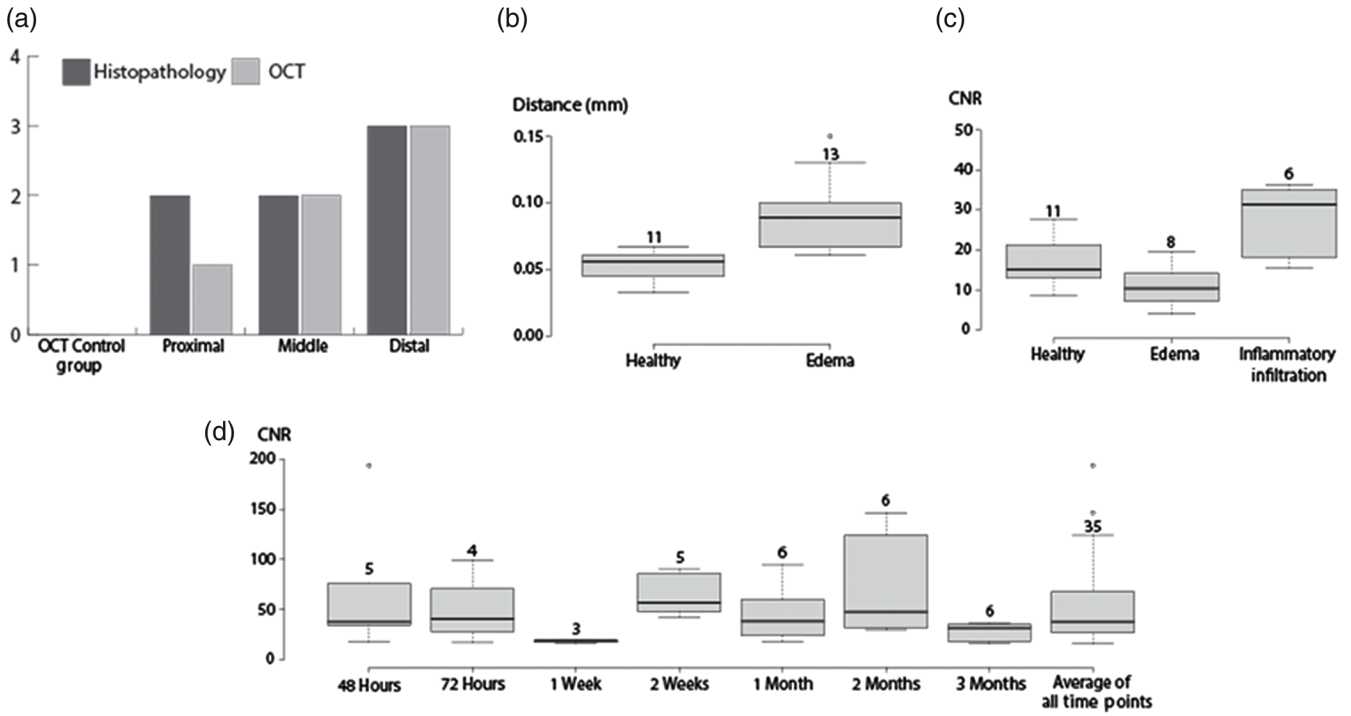

Fig. 9 (a) Number of inflammatory infiltration occurrences in histopathology and OCT as a function of dose (proximal, middle, and distal esophagus) after three months, as well as for the OCT control group. (b) These boxplots illustrate the differences in distance between the muscularis mucosa and lamina propria esophageal layers for healthy esophageal tissue (left) and edema (right). Boxes indicate interquartile ranges, horizontal lines illustrate the median values, the circles are outliners, and error bars represent the range. (c) Boxplot of CNR values for healthy esophageal wall, edema, and inflammatory infiltration after three months. (d) The boxplots show CNR values of inflammatory infiltration at several time-points postirradiation.

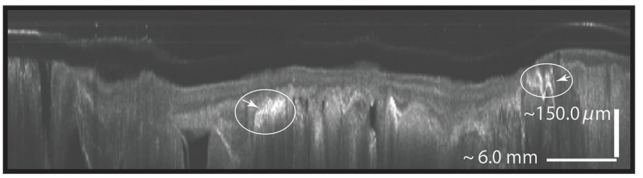

Fig. 10 *In vivo* OCT images of a mouse esophagus showing examples of high scattering areas that are present in almost all cases.

availability of dedicated OCT probes and esophageal OCT imaging systems, although damage may occur at other dose levels.[32,40,62]

In conclusion, we studied the feasibility of OCT to detect and monitor ARIED in a small animal model (mice). We irradiated the mice using single-dose delivery of 4.0, 10.0, 16.0, and 20.0 Gy on small spots. Inflammation was mostly seen at the highest dose region. Our results indicated the potential role of OCT to assess and monitor the ARIED in mice by detecting changes in light scattering in tissue and esophageal wall layer thicknesses, which may translate to humans.

Appendix

We evaluated the visibility of such damage quantitatively by calculating the CNR.[32] We defined CNR as the difference between the mean intensity of the selected region (inflammatory infiltration, edema, and healthy tissue) and the mean intensity of the background—as dark regions of the image—divided by the standard deviation of the background intensities as follows:[32]

$$\mathrm{CNR} = \frac{|\mathrm{MI}_{\mathrm{Region}} - \mathrm{MI}_{\mathrm{Background}}|}{\mathrm{SD}(\mathrm{I}_{\mathrm{Background}})},$$

where $\mathrm{MI}_{\mathrm{Region}}$ is the mean intensity of the identified region of interest (ROI) of 1.20 mm × 0.06 mm, $\mathrm{MI}_{\mathrm{Background}}$ is the mean intensity of the associated background ROI of 1.20 mm × 0.06 mm in the image, and $\mathrm{SD}(\mathrm{I}_{\mathrm{Background}})$ is defined as the standard deviation of the background intensities within the ROI of 1.2 mm × 0.06 mm. CNR measurements were performed using the open-source ImageJ software on raw data, guided by our visual findings in in-house developed software Worldmatch.[31]

We also measured the distance between the muscularis mucosa and lamina propria of edema and healthy esophageal tissues to evaluate the visibility of edema quantitatively. We used repeated measures ANOVA to evaluate the differences in CNR values between healthy tissue, edema, and inflammatory infiltration at different time-points and the differences between the muscularis mucosa and lamina propria distances in healthy and edema stages. We considered our findings significant when the one-sided p-value was <0.05 and visualized the results as boxplots with interquartile ranges.

Disclosures

Dr. T. Alderliesten is involved in projects supported by Elekta. Professor J. F. de Boer is a beneficiary of patents that are licensed to Ninepoint Medical, Inc. Elekta and NinePoint

Medical, Inc. had no involvement in the study design, the data collection, analysis and interpretation, and the writing of the paper.

Acknowledgments

This work was supported by The Netherlands Organization for Health and Development (ZonMw), Elekta Ltd., and NinePoint Medical, Inc. The authors would like to thank Dirk J. Faber for useful discussion. The authors would like to thank Marco Breuer, Koen van der Mark, and Roel Sneepers for their help with animal facility-related preparation and acknowledge Niels de Wit, Corine van Langen, Anouk Post, and Tanja Maidment for assisting with data acquisition.

References

1. J. Y. Chang et al., "Image-guided radiation therapy for non-small cell lung cancer," *J. Thorac. Oncol.* **3**(2), 177–186 (2008).
2. M. D. Fountain et al., "Radiation-induced esophagitis is mitigated by soy isoflavones," *Front. Oncol.* **5**, 238 (2015).
3. J. D. Lawson et al., "Frequency of esophageal stenosis after simultaneous modulated accelerated radiation therapy and chemotherapy for head and neck cancer," *Am. J. Otolaryngol.* **29**(1), 13–19 (2008).
4. E. Alevronta et al., "Dose-response relations for stricture in the proximal oesophagus from head and neck radiotherapy," *Radiother. Oncol.* **97**(1), 54–59 (2010).
5. M. Werner-Wasik et al., "Acute esophagitis and late lung toxicity in concurrent chemoradiotherapy trials in patients with locally advanced non-small-cell lung cancer: analysis of the Radiation Therapy Oncology Group (RTOG) database," *Clin. Lung Cancer* **12**(4), 245–251 (2011).
6. D. A. Palma et al., "Predicting esophagitis after chemoradiation therapy for non-small cell lung cancer: an individual patient data meta-analysis," *Int. J. Radiat. Oncol. Biol. Phys.* **87**(4), 690–696 (2013).
7. D. A. Palma et al., "Predicting radiation pneumonitis after chemoradiation therapy for lung cancer: an international individual patient data meta-analysis," *Int. J. Radiat. Oncol. Biol. Phys.* **85**(2), 444–450 (2013).
8. S. J. Ahn et al., "Dosimetric and clinical predictors for radiation-induced esophageal injury," *Int. J. Radiat. Oncol. Biol. Phys.* **61**(2), 335–347 (2005).
9. J. D. Cox, J. Stetz, and T. F. Pajak, "Toxicity criteria of the Radiation Therapy Oncology Group (RTOG) and the European Organization for Research and Treatment of Cancer (EORTC)," *Int. J. Radiat. Oncol. Biol. Phys.* **31**(5), 1341–1346 (1995).
10. S. Hirota et al., "Endoscopic findings of radiation esophagitis in concurrent chemoradiotherapy for intrathoracic malignancies," *Radiother. Oncol.* **58**(3), 273–278 (2001).
11. L. R. Coia, R. J. Myerson, and J. E. Tepper, "Late effects of radiation therapy on the gastrointestinal tract," *Int. J. Radiat. Oncol. Biol. Phys.* **31**(5), 1213–1236 (1995).
12. V. Bar Ad et al., "Treatment-related esophagitis for patients with locoregionally advanced non-small cell lung cancer treated with involved-field radiation therapy and concurrent chemotherapy," *Int. J. Radiat. Oncol.* **84**(3), S551–S552 (2012).
13. M. Werner-Wasik et al., "Radiation dose-volume effects in the esophagus," *Int. J. Radiat. Oncol. Biol. Phys.* **76**(3), S86–S93 (2010).
14. L. E. Court et al., "A technique to use CT images for in vivo detection and quantification of the spatial distribution of radiation-induced esophagitis," *J. Appl. Clin. Med. Phys.* **14**(3), 91–98 (2013).
15. J. Nijkamp et al., "Relating acute esophagitis to radiotherapy dose using FDG-PET in concurrent chemo-radiotherapy for locally advanced non-small cell lung cancer," *Radiother. Oncol.* **106**(1), 118–123 (2013).
16. A. K. Singh, M. A. Lockett, and J. D. Bradley, "Predictors of radiation-induced esophageal toxicity in patients with non-small-cell lung cancer treated with three-dimensional conformal radiotherapy," *Int. J. Radiat. Oncol. Biol. Phys.* **55**(2), 337–341 (2003).
17. D. Huang et al., "Optical coherence tomography," *Science* **254**, 1178–1181 (1991).
18. S. H. Yun et al., "Comprehensive volumetric optical microscopy in vivo," *Nat. Med.* **12**, 1429–1433 (2006).
19. H. C. Wolfsen et al., "Safety and feasibility of volumetric laser endomicroscopy in patients with Barrett's esophagus (with videos)," *Gastrointest. Endosc.* **82**, 631–640 (2015).
20. A. Swager et al., "Volumetric laser endomicroscopy in Barrett's esophagus: a feasibility study on histological correlation," *Dis. Esophagus* **29**(6), 505–512 (2016).
21. M. J. Suter et al., "Esophageal-guided biopsy with volumetric laser endomicroscopy and laser cautery marking: a pilot clinical study," *Gastrointest. Endosc.* **79**(6), 886–896 (2014).
22. V. Sun et al., "In vivo feasibility of endovascular Doppler optical coherence tomography," *Biomed. Opt. Express* **3**(10), 2600–2610 (2012).
23. M. T. J. Bus et al., "Volumetric in vivo visualization of upper urinary tract tumors using optical coherence tomography: a pilot study," *J. Urol.* **190**, 2236–2242 (2013).
24. P. Cernohorsky et al., "In-situ imaging of articular cartilage of the first carpometacarpal joint using co-registered optical coherence tomography and computed tomography," *J. Biomed. Opt.* **17**(6), 060501 (2012).
25. M. J. Gora et al., "Tethered capsule endomicroscopy enables less invasive imaging of gastrointestinal tract microstructure," *Nat. Med.* **19**(2), 238–240 (2013).
26. N. Tabatabaei et al., "Tethered confocal endomicroscopy capsule for diagnosis and monitoring of eosinophilic esophagitis," *Biomed. Opt. Express* **5**(1), 197–207 (2014).
27. M. Gora et al., "Tethered capsule endomicroscopy: from bench to bedside at a primary care practice," *J. Biomed. Opt.* **21**(10), 104001 (2016).
28. D. M. de Bruin et al., "Assessment of apoptosis induced changes in scattering using optical coherence tomography," *J. Biophotonics* **9**(9), 913–923 (2016).
29. G. van Soest et al., "Atherosclerotic tissue characterization in vivo by optical coherence tomography attenuation imaging," *J. Biomed. Opt.* **15**(1), 011105 (2010).
30. R. Clarkson et al., "Characterization of image quality and image-guidance performance of a preclinical microirradiator," *Med. Phys.* **38**(2), 845–856 (2011).
31. J. W. Wolthaus et al., "Fusion of respiration-correlated PET and CT scans: correlated lung tumour motion in anatomical and functional scans," *Phys. Med. Biol.* **50**(7), 1569–1583 (2005).
32. P. Jelvehgaran et al., "Visibility of fiducial markers used for image-guided radiation therapy on optical coherence tomography for registration with CT: an esophageal phantom study," *Med. Phys.* **44**(12), 6570–6582 (2017).
33. C. L. Shields et al., "Optical coherence tomography angiography of the macula after plaque radiotherapy of choroidal melanoma: comparison of irradiated versus nonirradiated eyes in 65 patients," *Retina* **36**(8), 1493–1505 (2016).
34. K. K. Veverka et al., "Noninvasive grading of radiation retinopathy," *Retina* **35**(11), 2400–2410 (2015).
35. A. Maeda et al., "In vivo optical imaging of tumor and microvascular response to ionizing radiation," *PLoS One* **7**(8), e42133 (2012).
36. B. Davoudi et al., "Optical coherence tomography platform for microvascular imaging and quantification: initial experience in late oral radiation toxicity patients," *J. Biomed. Opt.* **18**(7), 076008 (2013).
37. C. C. B. de Oliveira Mota et al., "Optical coherence tomography as an auxiliary tool for the screening of radiation-related caries," *Photomed. Laser Surg.* **31**(7), 301–306 (2013).
38. G. Farhat et al., "Optical coherence tomography spectral analysis for detecting apoptosis in vitro and in vivo," *J. Biomed. Opt.* **20**(12), 126001 (2015).
39. L. Y. Robles, S. Singh, and P. M. Fisichella, "Emerging enhanced imaging technologies of the esophagus: spectroscopy, confocal laser endomicroscopy, and optical coherence tomography," *J. Surg. Res.* **195**(2), 502–514 (2015).
40. A. Sergeev et al., "In vivo endoscopic OCT imaging of precancer and cancer states of human mucosa," *Opt. Express* **1**(13), 432–440 (1997).
41. B. Bouma and G. Tearney, "High-resolution imaging of the human esophagus and stomach in vivo using optical coherence tomography," *Gastrointest. Endosc.* **51**(4), 467–474 (2000).
42. C. Pitris et al., "Feasibility of optical coherence tomography for high-resolution imaging of human gastrointestinal tract malignancies," *J. Gastroenterol.* **35**(2), 87–92 (2000).

43. A. F. Swager et al., "Detection of buried Barrett's glands after radiofrequency ablation with volumetric laser endomicroscopy," *Gastrointest. Endosc.* **83**(1), 80–88 (2016).
44. M. J. Cobb et al., "Imaging of subsquamous Barrett's epithelium with ultrahigh-resolution optical coherence tomography: a histologic correlation study," *Gastrointest. Endosc.* **71**(2), 223–230 (2010).
45. J. M. Poneros et al., "Diagnosis of specialized intestinal metaplasia by optical coherence tomography," *Gastroenterology* **120**(1), 7–12 (2001).
46. G. Isenberg et al., "Accuracy of endoscopic optical coherence tomography in the detection of dysplasia in Barrett's esophagus: a prospective, double-blinded study," *Gastrointest. Endosc.* **62**(6), 825–831 (2005).
47. V. Demidov et al., "Preclinical longitudinal imaging of tumor microvascular radiobiological response with functional optical coherence tomography," *Sci. Rep.* **8**(1), 1–12 (2018).
48. A. V. Maslennikova et al., "In-vivo longitudinal imaging of microvascular changes in irradiated oral mucosa of radiotherapy cancer patients using optical coherence tomography," *Sci. Rep.* **7**(1), 16505 (2017).
49. B. Davoudi et al., "Noninvasive in vivo structural and vascular imaging of human oral tissues with spectral domain optical coherence tomography," *Biomed. Opt. Express* **3**(5), 826–839 (2012).
50. D. Murro and S. Jakate, "Radiation esophagitis," *Arch. Pathol. Lab. Med.* **139**, 827–830 (2015).
51. J. Overgaard et al., "Comparison of conventional and split-course radiotherapy as primary treatment in carcinoma of the larynx," *Acta Oncol.* **27**(2), 147–152 (1988).
52. H. P. Bijl et al., "Unexpected changes of rat cervical spinal cord tolerance caused by inhomogeneous dose distributions," *Int. J. Radiat. Oncol. Biol. Phys.* **57**(1), 274–281 (2003).
53. A. J. van der Kogel, "Late effects of radiation on the spinal cord," Radiobiological Institute TNO, Rijswijk, The Netherlands (1979).
54. Y. Niu et al., "Protection of esophageal multi-lineage progenitors of squamous epithelium (stem cells) from ionizing irradiation by manganese superoxide dismutase-plasmid/liposome (MnSOD-PL) gene therapy," *In Vivo* **19**(6), 965–974 (2005).
55. H. A. Gay et al., "Isodose-based methodology for minimizing the morbidity and mortality of thoracic hypofractionated radiotherapy," *Radiother. Oncol.* **91**(3), 369–378 (2009).
56. S. Adebahr et al., "Oesophagus side effects related to the treatment of oesophageal cancer or radiotherapy of other thoracic malignancies," *Best Pract. Res. Clin. Gastroenterol.* **30**(4), 565–580 (2016).
57. A. Niemierko and M. Goitein, "Modeling of normal tissue response to radiation," *Int. J. Radiat. Oncol. Biol. Phys.* **25**, 135–145 (1993).
58. N. Uribe-Patarroyo and B. E. Bouma, "Rotational distortion correction in endoscopic optical coherence tomography based on speckle decorrelation," *Opt. Lett.* **40**(23), 5518–5521 (2015).
59. Y. Kawase et al., "Comparison of nonuniform rotational distortion between mechanical IVUS and OCT using a phantom model," *Ultrasound Med. Biol.* **33**(1), 67–73 (2007).
60. W. Kang et al., "Motion artifacts associated with in vivo endoscopic OCT images of the esophagus," *Opt. Express* **19**(21), 20722–20735 (2011).
61. N. S. Van Ditzhuijzen et al., "The impact of Fourier-domain optical coherence tomography catheter induced motion artefacts on quantitative measurements of a PLLA-based bioresorbable scaffold," *Int. J. Cardiovasc. Imaging* **30**(6), 1013–1026 (2014).
62. G. J. Tearney et al., "In vivo endoscopic optical biopsy with optical coherence tomography," *Science* **276**(5321), 2037–2039 (1997).

Pouya Jelvehgaran is a PhD candidate in the Biomedical Engineering and Physics and Radiation Oncology Departments, the Academic Medical Center, the University of Amsterdam and LaserLaB Amsterdam. He received his MSc degree in medical engineering from KTH–Royal Institute of Technology, in a joint program with Karolinska Institutet, Sweden. The focus of his research is advanced optical imaging of the esophagus during cancer therapy, image-guided radiation therapy, optical coherence tomography, and translational research.

Daniel Martijn de Bruin is employed as a faculty member in the Department of Urology and the Department of Biomedical Engineering and Physics, the Academic Medical Center where he initiates translational research projects. He holds several grants, is a principal investigator of multiple research projects, is member of the EAU, AUA, SPIE and COST, and published over 100 papers covering optical and digital diagnostic imaging technologies and focal therapies of benign and malignant disease.

F. Javier Salguero is currently a senior programmer at the radiotherapy software Fratoria BV focusing in the development of Monte Carlo-based software solutions. He received his PhD from the University of Sevilla developing a Monte Carlo treatment planning system. After that, he was a postdoctoral researcher at the Virginia Commonwealth University and the Nederlands Kanker Instituut. His research focused in small animal radiotherapy and effect of radiation in healthy tissues and Monte Carlo simulations.

Gerben Roelof Borst is a radiation oncologist in the Department of Radiation Oncology and an assistant professor in the Division of Cell Biology, The Netherlands Cancer Institute, The Netherlands. His research focuses in clinical field: in the field of neuro-oncology, cranial and extra-cranial stereotactic radiotherapy, and response monitoring and prediction; preclinical research: dynamic changes during radiotherapy aiming to elucidate how to optimally target radioresistance; clinical research: the use of different imaging modalities and optimized image-guided radiotherapy in the field of neuro-oncology.

Ji-Ying Song received her MD degree and specialization in surgical pathology from Suzhou Medical College and at the Suzhou No. 1 Academic Hospital, China. She received her PhD from the Department of Cell Biology and Histology, the Academic Medical Center, the University of Amsterdam, The Netherlands. She was a postdoc at the Max-Planck-Institut für experimentelle Medizin, Molecular Neurobiology Department, Goettingen, Germany. She is the laboratory animal pathologist at The Netherlands Cancer Institute, Amsterdam, The Netherlands.

Ton G. van Leeuwen is a full professor in biomedical physics and in 2008 was appointed as the head of the Biomedical Engineering and Physics Department, the Academic Medical Center, the University of Amsterdam. His current research focuses on the physics of the interaction of light with tissue and using that knowledge for the development, introduction, and clinical evaluation of newly developed optical imaging techniques for gathering quantitative functional and molecular information of tissue.

Johannes F. de Boer is a full professor in the Department of Physics and Astronomy, VU University, Amsterdam and a former director of LaserLaB Amsterdam. He has been an active researcher in biomedical optics for over 20 years since obtaining his PhD from the University of Amsterdam. He was an assistant professor at the Beckman Laser Institute, UC Irvine, California, and an associate professor at Harvard Medical School, Boston, Massachusetts. He has ~140 peer-reviewed papers and an H-index of 55 (Web of Science).

Tanja Alderliesten received her PhD in computer science from the Utrecht University, The Netherlands, in 2004. Currently, she is a tenured senior researcher in the Department of Radiation Oncology, the Academic Medical Center, The Netherlands. The focus of her research is on translational research and development of state-of-the-art methods and techniques from the field of mathematics and computer science (including image processing, biomedical modeling, and optimization) to radiation oncology.

Marcel van Herk is a professor of radiotherapy physics in Manchester. This is a joint post between the University of Manchester and the Christie. He is responsible for developing a program of international leading radiotherapy physics research and innovation to deliver direct patient benefits. The main focus is on accuracy of radiotherapy, including target volume definition, treatment planning, image guidance, and treatment follow-up. Among others, he was the main developer of cone-beam CT-guided radiotherapy.